An E3 Ligase Possessing an Iron-Responsive Hemerythrin Domain Is a Regulator of Iron Homeostasis

Ameen A. Salahudeen,* Joel W. Thompson,* Julio C. Ruiz, He-Wen Ma, Lisa N. Kinch, Qiming Li, Nick V. Grishin, Richard K. Bruick†

Cellular iron homeostasis is maintained by the coordinate posttranscriptional regulation of genes responsible for iron uptake, release, use, and storage through the actions of the iron regulatory proteins IRP1 and IRP2. However, the manner in which iron levels are sensed to affect IRP2 activity is poorly understood. We found that an E3 ubiquitin ligase complex containing the FBXL5 protein targets IRP2 for proteasomal degradation. The stability of FBXL5 itself was regulated, accumulating under iron- and oxygen-replete conditions and degraded upon iron depletion. FBXL5 contains an iron- and oxygen-binding hemerythrin domain that acted as a ligand-dependent regulatory switch mediating FBXL5's differential stability. These observations suggest a mechanistic link between iron sensing via the FBXL5 hemerythrin domain, IRP2 regulation, and cellular responses to maintain mammalian iron homeostasis.

Although iron is an essential cofactor for many proteins, its chemical properties also promote side reactions that damage macromolecules. Failure to maintain proper iron homeostasis can lead to a variety of diseases including anemia and iron overload disorders (*1*–*4*). When cellular iron bioavailability is low, the iron regulatory proteins IRP1 and IRP2 coordinate the posttranscriptional regulation of many genes affecting cellular and systemic iron homeostasis by binding to iron response elements (IREs) found within their mRNAs (*5*, *6*). For example, when IRPs bind to the IRE located within the 5′ untranslated region (UTR) of the ferritin mRNA, initiation of protein synthesis is repressed (*1*, *2*). Conversely, IRP binding to IREs within the transferrin receptor 1 (TfR1) 3′UTR stabilizes the mRNA and increases its expression (*7*). When cellular iron bioavailability is high, IRP1 assembles an iron-sulfur cluster and loses its affinity for IREs (*6*), whereas IRP2 is preferentially degraded by the proteasome (*8*, *9*). However, the underlying mechanism(s) by which cells directly sense iron (as well as oxygen) bioavailability and relate those changes to differences in IRP2 stability remain controversial (*10*–*15*).

To address these questions, we performed a small interfering RNA (siRNA) screen to identify an E3 ubiquitin ligase that regulates IRP2 stability (*16*). A clonal human embryonic kidney (HEK)

Department of Biochemistry, University of Texas Southwestern Medical Center, Dallas, TX 75390, USA.

*These authors contributed equally to this work.
†To whom correspondence should be addressed. E-mail: richard.bruick@utsouthwestern.edu

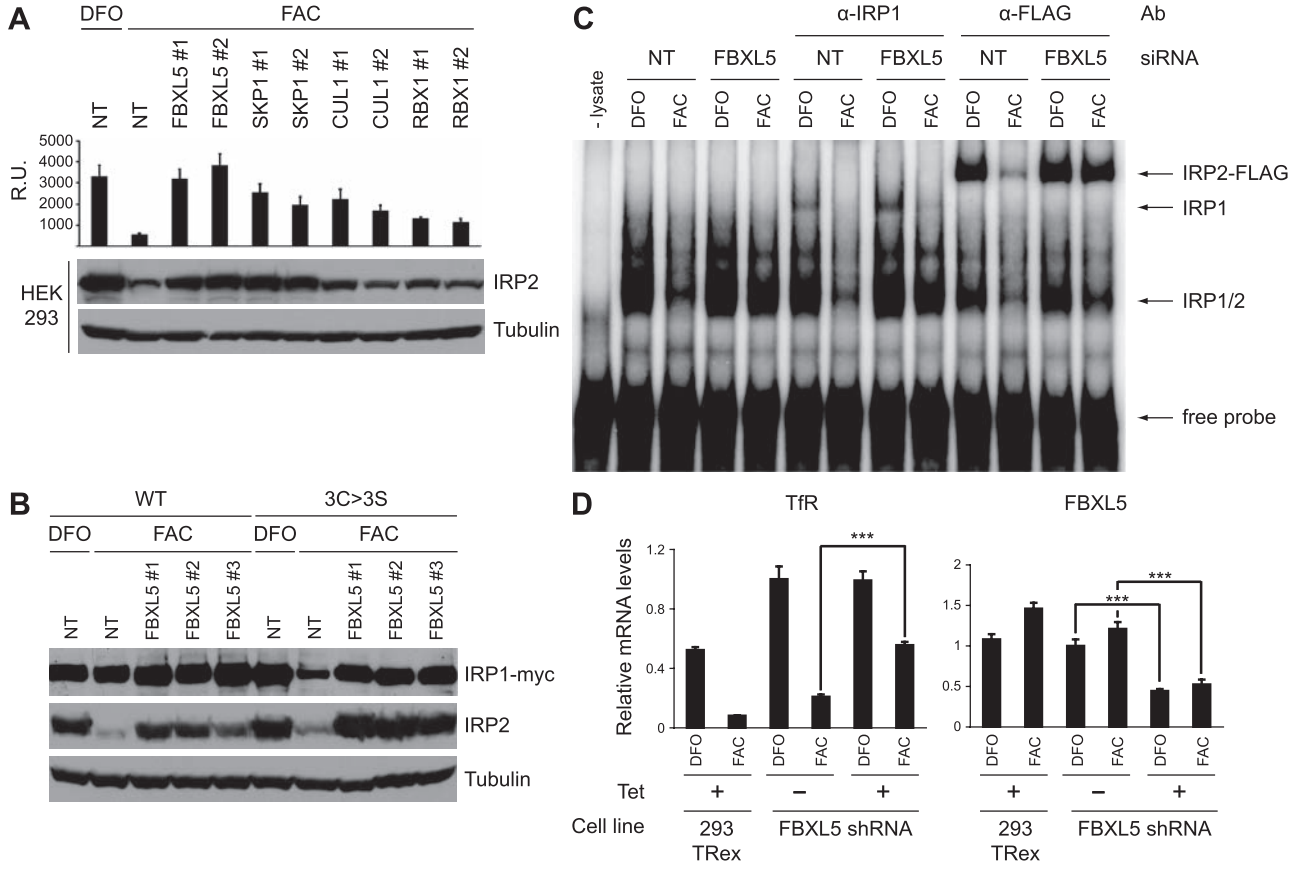

Fig. 1. IRP2 is stabilized under iron-replete conditions after siRNA-mediated suppression of SCF^{FBXL5}. (**A**) IRP2 accumulation was assessed using the AlphaScreen assay (top) or by immunoblot analysis of endogenous IRP2 (bottom). Knockdown efficiency of the SKP1, CUL1, and RBX1 siRNAs is shown in fig. S2D. (**B**) IRP1 stabilization under iron-replete conditions after siRNA-mediated suppression of FBXL5, as measured by immunoblot analysis of HEK 293 cell lines stably transfected with either a myc-tagged wild-type (WT) or 3C>3S IRP1 Tet-inducible expression construct. (**C**) Measurement of RNA binding activity from lysates after siRNA-mediated suppression of FBXL5 in cells expressing HA-IRP2-FLAG. Because human IRP1-IRE and IRP2-IRE complexes migrate similarly, antibodies were added to supershift individual complexes. (**D**) Relative TfR1 and FBXL5 mRNA accumulation levels measured by qRT-PCR. Assays were performed in triplicate with data represented as the mean ± SE with *P* values determined using Student's unpaired *t* test (****P* < 0.001).

293 cell line stably transfected with a plasmid constitutively expressing N-terminal hemagglutinin (HA)–tagged and C-terminal FLAG-tagged IRP2 accumulated high levels of HA-IRP2-FLAG in cells depleted of iron upon treatment with the chelator deferoxamine mesylate (DFO). As observed for endogenous IRP2, low levels of HA-IRP2-FLAG accumulated in cells incubated in the presence of excess iron [ferric ammonium citrate (FAC); fig. S1B]. As an alternative to immunoblots, HA-IRP2-FLAG accumulation levels could be assessed using a high-throughput luminescent proximity assay (AlphaScreen; fig. S1A).

Inappropriate accumulation of HA-IRP2-FLAG under iron-replete conditions, consistent with reduced E3 ligase activity, was best observed with siRNAs targeting expression of the F-box–containing FBXL5 protein (*17*). Compared with a nontargeting (NT) control siRNA, knockdown of FBXL5 expression by either of two independent siRNAs (FBXL5 1 or 2) led to complete stabilization of HA-IRP2-FLAG under iron-replete conditions (Fig. 1A). Similar results were observed for endogenous IRP2 in HEK 293 cells (Fig. 1A), HeLa cells (fig. S2A), nontumorigenic HBEC-30 cells (fig. S2B), and a clonal cell line containing a tetracycline (Tet)–inducible FBXL5 short hairpin RNA (shRNA) (see below). F-box–containing proteins typically assemble within SCF E3 ubiquitin ligase complexes containing SKP1, Cullin 1 (CUL1), and RBX1 (*18*), each of which were also identified in the unbiased siRNA screen and whose knockdown partially stabilized IRP2 (Fig. 1A).

Despite a greater than 60% amino acid identity, IRP1 and IRP2 are regulated differently. Such differences are not attributable to the 73–amino acid insert unique to IRP2 (*19*), as deletion of this region does not preclude iron-dependent IRP2 degradation or sensitivity to FBXL5 knockdown (fig. S2C). Moreover, when IRP1 is not bound to an iron-sulfur cluster, it can be targeted for proteasomal degradation under iron-replete conditions, similar to IRP2 (*20*, *21*). Although little change in IRP1 levels was observed in FAC-treated HEK 293 cell lines stably expressing myc-tagged wild-type (WT) IRP1 after transfection with three independent FBXL5 siRNAs, a myc-tagged IRP1 (3C > 3S) lacking three cysteines required for Fe-S cluster assembly (*20*) responded in an analogous manner to endogenous IRP2 (Fig. 1B). Together, these data suggest that FBXL5 can recognize both apo-IRP1 and IRP2, likely through a common element.

We performed electrophoretic mobility shift assays to demonstrate that this accumulated IRP2 upon FBXL5 knockdown is functional. Knockdown of FBXL5 expression under iron-replete conditions increased total IRE binding activity (IRP1/2) to levels similar to those observed under iron-deficient conditions (Fig. 1C). Although IRP1's RNA binding activity is sensitive to cellular iron availability, FBXL5 knockdown had little effect on IRP1's IRE binding activity, which suggests that it does not simply reduce cellular iron uptake or availability. In contrast, the increased IRP2-FLAG levels upon FBXL5 knockdown in FAC-treated cells elevated total IRP2 RNA binding activity (Fig. 1C). Furthermore, in Tet-inducible FBXL5 shRNA cells, loss of FBXL5 expression (+Tet) resulted in a factor of ~2.5 increase in TfR1 mRNA accumulation under iron-replete conditions (Fig. 1D) consistent with the increased IRP2 levels (see below). Thus, reduced FBXL5 expression results in inappropriate accumulation of IRP2 under iron-replete conditions and increased IRP2 IRE binding activity with concomitant misregulation of IRP target genes.

A physical interaction between FBXL5 and IRP2 was observed as antibodies to FLAG coimmunoprecipitated FBXL5-V5 with IRP2-FLAG (Fig. 2A) and FLAG-tagged FBXL5 coimmunoprecipitated endogenous IRP2 (Fig. 2B). To investigate whether this interaction reflected an E3 ligase–substrate relationship, we prepared recombinant SCF^{FBXL5}. Affinity-purified FLAG-tagged WT FBXL5, but not FBXL5 lacking the F-box domain, assembled into a stoichiometric (fig. S3, A and B) SCF^{FBXL5} complex (Fig. 2C). Purified SCF^{FBXL5}, but not the ΔF-box FBXL5 variant (fig. S3C), was able to ubiquitinate recombinant IRP2 in vitro (Fig. 2D).

To reveal the mechanism by which SCF^{FBXL5} targets IRP2 for degradation in both an iron- and oxygen-dependent manner (*2*, *6*), we conducted an immunoblot analysis, which revealed that both FBXL5-FLAG (Fig. 3A) and endogenous FBXL5 (Fig. 3C) protein levels were low when iron is limiting but increased by more than an order of magnitude under iron-replete conditions. This difference was attenuated by addition of the proteasome inhibitor MG132 (Fig. 3A). Interestingly, FBXL5-FLAG protein levels were inversely regulated with respect to IRP2 (Fig. 3B). Because FBXL5 mRNA levels did not change significantly as a function of iron (Fig. 1D) and iron-dependent regulation of exogenous FBXL5-FLAG did not require elements from the FBXL5 promoter or UTRs, these data indicate that FBXL5 is posttranslationally targeted for proteasomal degradation in an iron-dependent manner. FBXL5-FLAG levels from iron-replete cells were also substantially lower when incubated under low-O_2 conditions (Fig. 3D). Thus, both

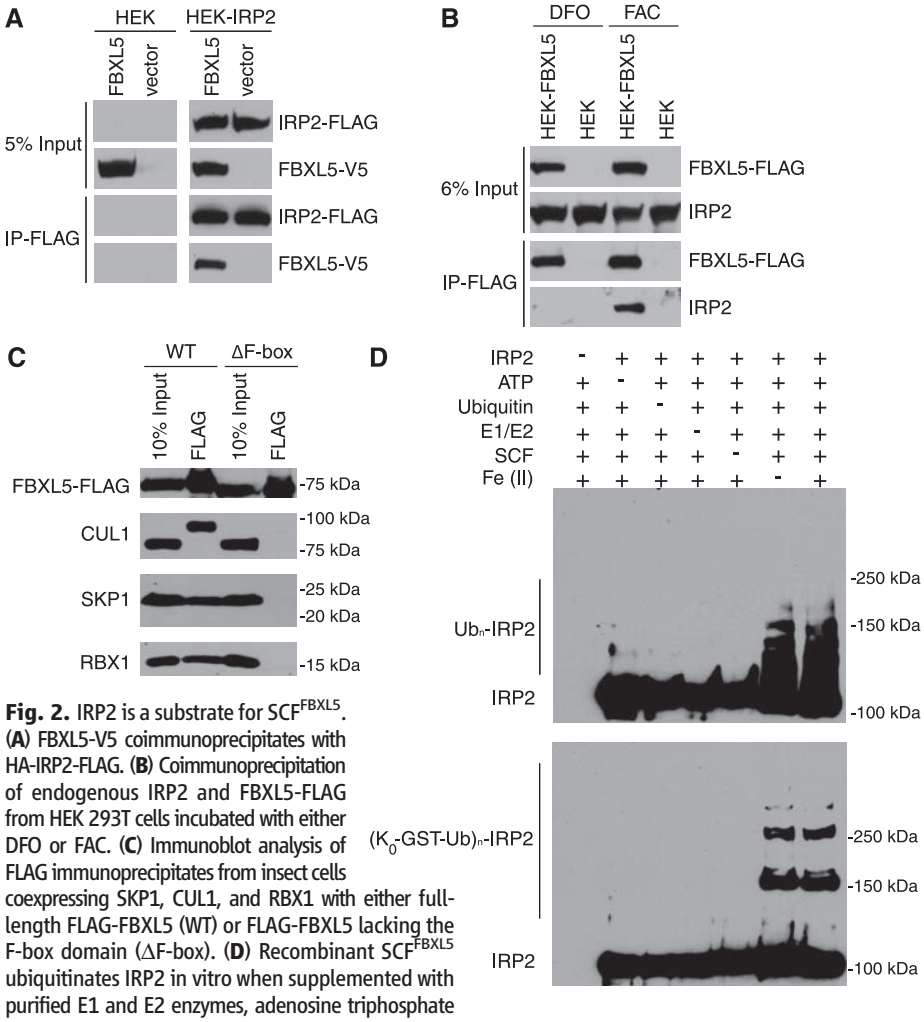

Fig. 2. IRP2 is a substrate for SCF^{FBXL5}. (**A**) FBXL5-V5 coimmunoprecipitates with HA-IRP2-FLAG. (**B**) Coimmunoprecipitation of endogenous IRP2 and FBXL5-FLAG from HEK 293T cells incubated with either DFO or FAC. (**C**) Immunoblot analysis of FLAG immunoprecipitates from insect cells coexpressing SKP1, CUL1, and RBX1 with either full-length FLAG-FBXL5 (WT) or FLAG-FBXL5 lacking the F-box domain (ΔF-box). (**D**) Recombinant SCF^{FBXL5} ubiquitinates IRP2 in vitro when supplemented with purified E1 and E2 enzymes, adenosine triphosphate (ATP), and WT ubiquitin (top) or glutathione *S*-transferase (GST)–tagged ubiquitin lacking lysines (K_0-GST-Ub) and thus unable to form polyubiquitin chains (bottom).

iron- and O_2-dependent regulation of IRP2 may be mediated by reciprocal effects on FBXL5's stability.

To identify the region of FBXL5 that confers such regulation, we transfected a series of V5-tagged FBXL5 deletion mutants (fig. S4) into HEK 293T cells followed by incubation with DFO or FAC. As observed for the full-length protein, all but one deletion construct showed preferential accumulation under conditions of excess iron. In contrast, the FBXL5 ΔN-term protein accumulated at constitutively high levels under both conditions (Fig. 3E). Moreover, expression of FBXL5 residues 1 to 161 demonstrated that this region was sufficient to recapitulate iron-dependent degradation (Fig. 3F).

Residues 1 to 161 of the human FBXL5 protein are predicted to contain five α helices encompassing several conserved histidine and glutamic acid residues (figs. S5 and S6A), similar to hemerythrin-like four-helix up and down bundles with an additional C-terminal helix packed against the core (fig. S6B). Although not previously reported in mammalian proteins, hemerythrin domains have been frequently reported to contain μ-oxo diiron centers (*22*) that reversibly bind oxygen (fig. S6C) and often function as O_2-transport proteins, O_2 sensors, or metal storage depots in marine invertebrates and bacteria (*23*). Recombinantly expressed (fig. S6D) FBXL5 hemerythrin domain (WT) copurified with iron, whereas mutation of one of the predicted bridging carboxylates (E61A) was sufficient to abolish iron binding (Fig. 4A). UV-visible absorbance spectroscopy of the WT domain also showed a broad absorbance peak around 330 nm, characteristic of oxidized μ-oxo diiron centers in hemerythrins (*24*), that decreased upon reduction with dithionite to remove oxygen (Fig. 4B). Circular dichroism spectrometry showed that the WT domain is largely α-helical with minima at 207 and 222 nm (*25*). In contrast, the spectrum of the E61A mutant is indicative of an unstructured protein (Fig. 4C). Thermal denaturation experiments (Fig. 4D) revealed that treatment of the hemerythrin domain with dithionite and the iron chelator *o*-phenanthroline lowers both the melting temperature and cooperativity of unfolding, which indicates that these reagents destabilize the tertiary fold of the domain (*25*). Thus, the FBXL5 N terminus folds into an α helix–rich structure capable of binding both iron and oxygen.

To determine whether the FBXL5 hemerythrin (Hr) domain could regulate a heterologous protein, we transfected HEK 293T cells with constructs expressing the domain fused to either the N terminus (Hr-Luc) or C terminus (Luc-Hr) of firefly luciferase. Unlike unmodified luciferase (Luc), both Hr-Luc (~2.5x) and Luc-Hr (~2.0x) luciferase activities were higher in lysates from FAC-treated cells and correlated with changes in fusion protein accumulation (Fig. 4E). Incubation under low-oxygen conditions also reduced fusion protein luciferase activity and accumulation under iron-replete conditions (Fig. 4E).

Because deletion of the hemerythrin domain resulted in constitutive FBXL5 accumulation (Δ1-161; Fig. 4F) and fusion of the domain conferred iron- and O_2-dependent regulation of stability in the context of a heterologous protein (Fig. 4E), a recognition motif for an E3 ubiquitin ligase (degron) likely resides within this domain. Several F-box proteins mediate their own stability through autoubiquitination (*26*), which may contribute to the partial stabilization of the ΔF-box variant (Fig. 3E). However, knockdown of FBXL5 expression has no effect on the iron-dependent accumulation of the hemerythrin domain itself (fig. S7), indicating that its degron is likely recognized by an as yet unidentified E3 ligase. In the folded iron- and oxygen-bound state, this degron may be efficiently sequestered from the E3 ligase within the hemerythrin fold, promoting FBXL5 accumulation and subsequent IRP2 degradation.

If the hemerythrin domain is unable to assemble a diiron center (e.g., iron-deficient conditions), the domain may unfold to reveal the degron. Degradation of FBXL5 would then preclude the assembly of the SCF complex allowing IRP2 to

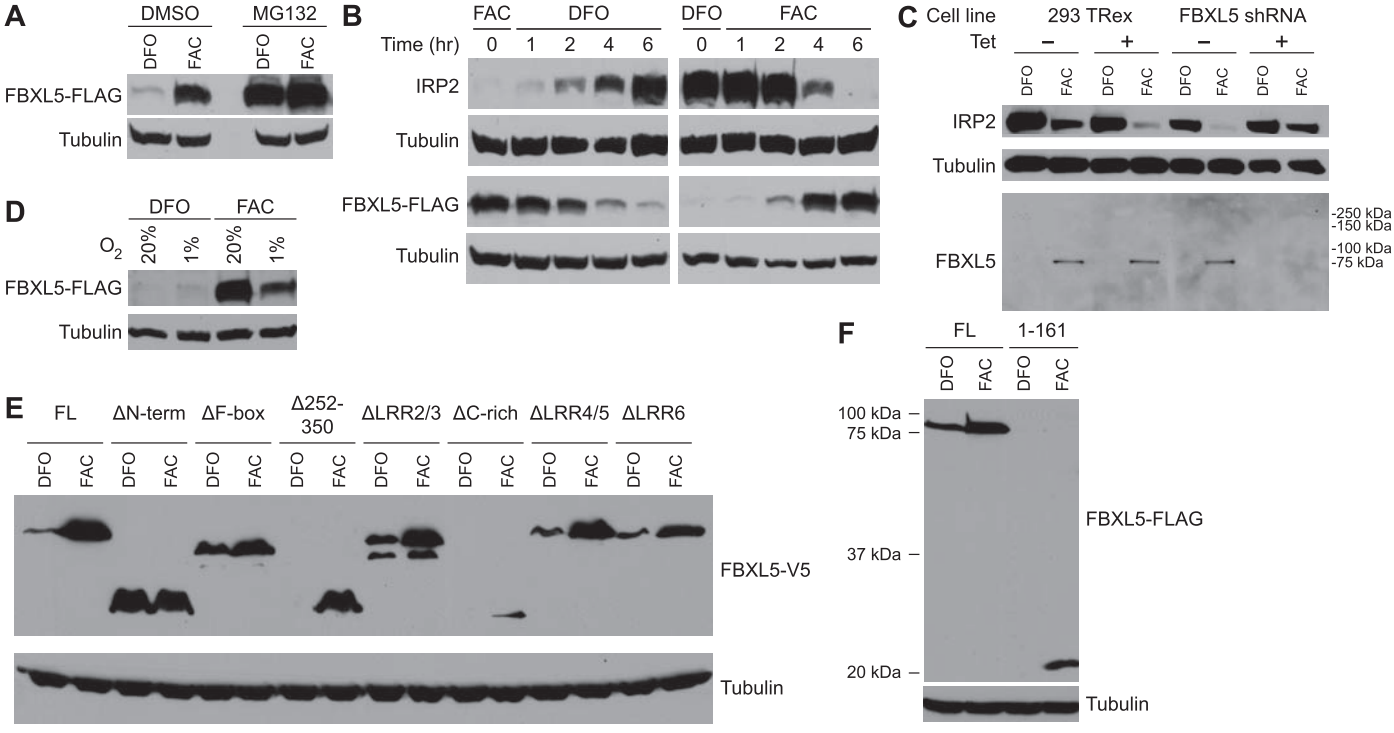

Fig. 3. FBXL5 protein accumulation is dependent on iron and oxygen availability. (**A**) Immunoblot analysis of stably transfected FBXL5-FLAG protein accumulation under iron-deplete (DFO) or iron-replete (FAC) conditions. (**B**) Time course of IRP2 and FBXL5 responses to changes in iron availability. HEK FBXL5-FLAG cells were incubated 16 hours with either FAC or DFO, then switched to low- or high-iron conditions, respectively. Quantitation is provided in table S1. (**C**) Endogenous IRP2 and FBXL5 levels were assessed by immunoblot analysis in WT cells (293 TRex) or in a clonal cell line stably expressing a Tet-inducible FBXL5 shRNA. (**D**) Accumulation of FBXL5 under iron-replete conditions is attenuated (by a factor of 2.5) in cells incubated under low-oxygen conditions (1% O_2) for 16 hours. (**E** and **F**) Residues 1 to 161 mediate iron- and oxygen-dependent regulation of FBXL5 accumulation. Assessment of FBXL5 protein accumulation under iron-deplete (DFO) or iron-replete (FAC) conditions by immunoblot analysis of transiently transfected FBXL5 constructs. Quantitation is provided in table S2.

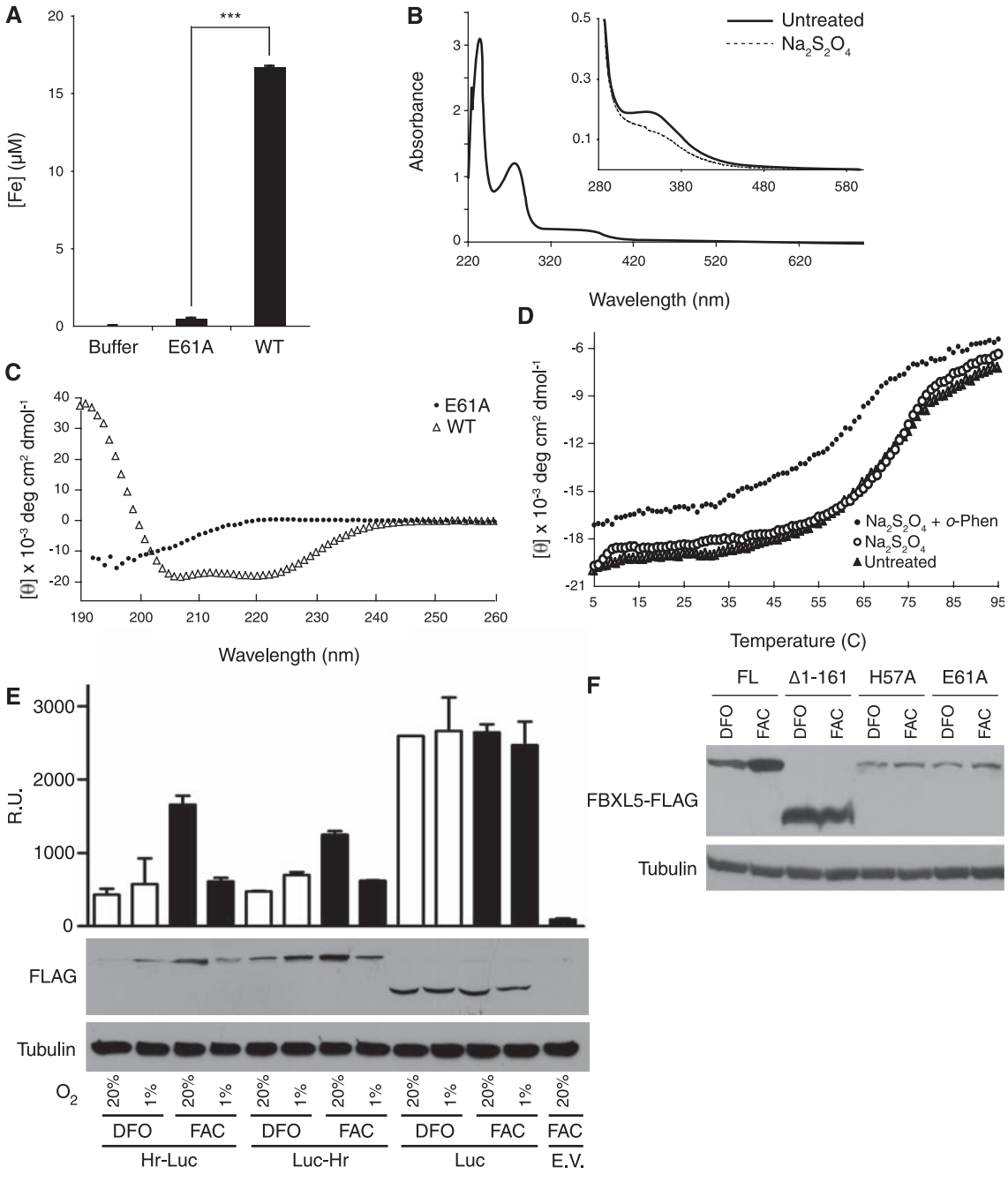

Fig. 4. FBXL5 contains an iron- and oxygen-binding hemerythrin domain that regulates its stability. (**A**) Iron content of recombinant WT or variant (E61A) FBXL5 hemerythrin domains. Assays were performed in triplicate with data represented as the mean ± SE, with *P* values determined using Student's unpaired *t* test (***$P < 0.001$). (**B**) UV chromatogram of the FBXL5 hemerythrin domain before and after dithionite addition. (**C**) Circular dichroism spectra of purified FBXL5 hemerythrin domains. (**D**) Measurement of mean molar residual ellipticity at 222 nm as a function of thermal denaturation of the WT domain treated with dithionite and iron chelator (*o*-Phen). (**E**) Luciferase activity (upper panels) and protein accumulation levels (lower panels; quantitation provided in table S3) in HEK 293T cells transiently transfected with fusion protein expression constructs. E.V., empty vector. Assays were performed in triplicate with data represented as the mean ± SE. (**F**) Immunoblot analysis of protein accumulation from transiently transfected FBXL5 expression constructs.

accumulate and bind IREs. Indeed, prior studies have implicated the involvement of such a labile protein in IRP2 degradation (*8*). Consistent with this model, mutation of iron-binding ligands prevented FBXL5 accumulation (Fig. 4F), suggesting an iron-insensitive, and unfolded, hemerythrin domain in which the degron is constitutively exposed. In contrast, ΔN-term FBXL5 overexpression partially circumvented iron-dependent IRP2 regulation, as observed by a reduction of IRP2 accumulation under iron-deplete conditions (fig. S8). However, the inability of ΔN-term FBXL5 overexpression to fully block IRP2 accumulation in DFO-treated cells may indicate the presence of additional mechanism(s) by which iron and oxygen regulate SCF^{FBXL5}. Underscoring this possibility is the observation that FBXL5 and IRP2 failed to coimmunoprecipitate in lysates from DFO-treated cells, which suggests that iron availability may also affect substrate recognition (Fig. 2B). We did not observe a further increase in ubiquitination activity when additional iron was added to recombinant SCF^{FBXL5} in vitro (Fig. 2D), which suggests two possibilities: Either there was sufficient iron present during purification, or the minimal reconstitution assay presented here did not fully recapitulate all aspects of SCF^{FBXL5} regulation.

Like several F-box–containing proteins reported to act as ligand-regulated effector proteins in plants (*27*), FBXL5 is an example of a ligand-regulated F-box protein in metazoans. Our observations suggest a direct mechanistic link between sensing iron and oxygen availability via FBXL5's hemerythrin domain, IRP2 induction, and the regulation of mammalian iron homeostasis.

References and Notes

1. M. U. Muckenthaler, B. Galy, M. W. Hentze, *Annu. Rev. Nutr.* **28**, 197 (2008).
2. M. L. Wallander, E. A. Leibold, R. S. Eisenstein, *Biochim. Biophys. Acta* **1763**, 668 (2006).
3. E. Beutler, *Annu. Rev. Med.* **57**, 331 (2006).
4. D. M. Wrighting, N. C. Andrews, *Curr. Top. Dev. Biol.* **82**, 141 (2008).
5. M. W. Hentze, M. U. Muckenthaler, N. C. Andrews, *Cell* **117**, 285 (2004).
6. T. A. Rouault, *Nat. Chem. Biol.* **2**, 406 (2006).
7. D. M. Koeller *et al.*, *Proc. Natl. Acad. Sci. U.S.A.* **86**, 3574 (1989).

8. B. Guo, J. D. Phillips, Y. Yu, E. A. Leibold, *J. Biol. Chem.* **270**, 21645 (1995).
9. F. Samaniego, J. Chin, K. Iwai, T. A. Rouault, R. D. Klausner, *J. Biol. Chem.* **269**, 30904 (1994).
10. K. Iwai *et al.*, *Proc. Natl. Acad. Sci. U.S.A.* **95**, 4924 (1998).
11. K. Yamanaka *et al.*, *Nat. Cell Biol.* **5**, 336 (2003).
12. E. Bourdon *et al.*, *Blood Cells Mol. Dis.* **31**, 247 (2003).
13. E. S. Hanson, M. L. Rawlins, E. A. Leibold, *J. Biol. Chem.* **278**, 40337 (2003).
14. J. Wang *et al.*, *Mol. Cell. Biol.* **24**, 954 (2004).
15. K. B. Zumbrennen, E. S. Hanson, E. A. Leibold, *Biochim. Biophys. Acta* **1783**, 246 (2008).
16. See supporting material on *Science* Online.
17. N. Zhang *et al.*, *Biochem. Biophys. Res. Commun.* **359**, 34 (2007).
18. A. R. Willems, M. Schwab, M. Tyers, *Biochim. Biophys. Acta* **1695**, 133 (2004).
19. K. Iwai, R. D. Klausner, T. A. Rouault, *EMBO J.* **14**, 5350 (1995).
20. S. L. Clarke *et al.*, *EMBO J.* **25**, 544 (2006).
21. C. Fillebeen, D. Chahine, A. Caltagirone, P. Segal, K. Pantopoulos, *Mol. Cell. Biol.* **23**, 6973 (2003).
22. R. E. Stenkamp, *Chem. Rev.* **94**, 715 (1994).
23. C. E. French, J. M. Bell, F. B. Ward, *FEMS Microbiol. Lett.* **279**, 131 (2008).
24. J. H. Zhang, D. M. Kurtz Jr., Y. M. Xia, P. G. Debrunner, *Biochemistry* **30**, 583 (1991).
25. N. J. Greenfield, *Nat. Protocols* **1**, 2876 (2007).
26. J. M. Galan, M. Peter, *Proc. Natl. Acad. Sci. U.S.A.* **96**, 9124 (1999).
27. D. E. Somers, S. Fujiwara, *Trends Plant Sci.* **14**, 206 (2009).

28. We thank R. Eisenstein for IRP1 reagents and helpful discussions; Z. Chen for SCF expression plasmids; W. Gao for K_0-GST-Ubiquitin and helpful discussions; M. Brown and J. Goldstein for E2 expression constructs; K. Gardner and F. Correa for assistance with circular dichroism; the UTSW HTS facility for assistance with siRNA screening; and L. Wang, G. Pineda, S. Laxman, X. Du, and J. Wang for helpful discussions. R.K.B. is the Michael L. Rosenberg Scholar in Medical Research and was supported by the Burroughs Wellcome Fund, the Robert A. Welch Foundation, the Texas Advanced Research Program, and NIH grant CA115962. This investigation was conducted in a facility constructed with support from the Research Facilities Improvement Program (grant C06 RR 15437-01) from the NIH National Center for Research Resources.

Supporting Online Material

www.sciencemag.org/cgi/content/full/1176326/DC1
Materials and Methods
Figs. S1 to S8
Tables S1 to S6
References

14 May 2009; accepted 26 August 2009
Published online 17 September 2009;
10.1126/science.1176326
Include this information when citing this paper.

Quantifying the Impact of Immune Escape on Transmission Dynamics of Influenza

Andrew W. Park,[1,2]* Janet M. Daly,[3,4] Nicola S. Lewis,[3,5,6] Derek J. Smith,[5,7,8] James L. N. Wood,[6] Bryan T. Grenfell[7,9,10]

Influenza virus evades prevailing natural and vaccine-induced immunity by accumulating antigenic change in the haemagglutinin surface protein. Linking amino acid substitutions in haemagglutinin epitopes to epidemiology has been problematic because of the scarcity of data connecting these scales. We use experiments on equine influenza virus to address this issue, quantifying how key parameters of viral establishment and shedding increase the probability of transmission with genetic distance between previously immunizing virus and challenge virus. Qualitatively similar patterns emerge from analyses based on antigenic distance and from a published human influenza study. Combination of the equine data and epidemiological models allows us to calculate the effective reproductive number of transmission as a function of relevant genetic change in the virus, illuminating the probability of influenza epidemics as a function of immunity.

As well as occasional pandemics caused by novel virus subtypes against which the population has no natural immunity, influenza virus causes annual epidemics in man, resulting in considerable morbidity and mortality (*1*). The recurring dynamics of annual influenza arises largely from the evolution of the virus (*2*) [particularly gradual changes in the surface antigens, haemagglutinin (HA), and neuraminidase, which determine the influenza subtype]. The mutation rate of the H3N2 subtype of human influenza A virus, which has caused most morbidity and mortality between 1968 and 2009, results in the appearance of antigenically novel viruses every 2 to 5 years (*3*). These viruses have amino acid substitutions at key antigenic sites, allowing them to escape the humoral immunity of individuals vaccinated or infected with preceding strains.

Integration of the epidemiological and evolutionary dynamics (phylodynamics) of influenza viruses is much studied (*3*–*7*). However, a crucial gap in our knowledge is that we do not know how changes in viral HA translate into immune escape in previously infected or vaccinated hosts, in terms of increases in the effective reproductive number (*8*). To quantify this relationship, we need data from controlled seasonal influenza infections, preferably of a natural mammalian host with manipulated prior immunity. A series of experimental infection studies with equine influenza virus (EIV) provides this opportunity (table S1).

Equine influenza vaccines have been used, particularly in racehorses, since the 1960s. For more than 40 years, all equine influenza infections have been caused by strains of the H3N8 subtype, which has a similar course of infection to seasonal influenza A in humans (*9*). In the late 1980s, and in contrast to influenza A in humans, the equine H3N8 subtype diverged into two lineages (*10*). Experiments in which homologous and heterologous equine influenza vaccines were tested (*11*) allow us to relate the impact of differences between vaccine and challenge strains on key epidemiological parameters. We begin with the simplest model, using amino acid substitutions (genetic distance) to measure heterology of different strain pairs (*11*). Our focus here is on relating broad patterns of heterology to epidemic risk. Outbreaks can occur in a wholly susceptible population when the basic reproductive number (R_0) exceeds one; that is, an infectious individual gives rise, on average, to more than one new infection (*8*). In populations that are not wholly susceptible (for example, a partially vaccinated population), the effective reproductive number, R, which takes into account that infectious individuals may make contact with nonsusceptible individuals, is the more appropriate measure of outbreak risk (*8*). The effective reproductive number can be calculated as $R = R_0\,pqd\,/\,d_{max}$, where p and q are the probabilities of becoming infected and infectious, respectively, and d is the infectious period (*11*). The parameter d_{max} is the maximum infectious period (estimated as the sample mean of the control animals).

The equine data (Fig. 1) show that even when the HAs of the vaccine and challenge strains are identical, the nonadjuvanted vaccines used are imperfect; animals vaccinated with a homologous strain have ~55% chance of becoming infected (p) and, if infected, have ~65% chance of becoming infectious (q), and are infectious (d) for an average of 2.8 days. Figure 1 also shows that p, q, and d increase with increasing number of amino acid differences in antigenic sites, a [supported by regression analyses (table S2)]. For mismatches of five or more amino acids in

[1]Odum School of Ecology, University of Georgia, Athens, GA 30602, USA. [2]Department of Infectious Diseases, College of Veterinary Medicine, University of Georgia, Athens, GA 30602, USA. [3]Animal Health Trust, Lanwades Park, Newmarket, Suffolk CB8 7UU, UK. [4]School of Veterinary Medicine and Science, The University of Nottingham, Sutton Bonington, Leicestershire LE12 5RD, UK. [5]Department of Zoology, University of Cambridge CB2 3EJ, UK. [6]Cambridge Infectious Diseases Consortium, Department of Veterinary Medicine, Cambridge CB3 0ES, UK. [7]Fogarty International Center, National Institutes of Health, Bethesda, MD 20892, USA. [8]Department of Virology, Erasmus Medical Center, Rotterdam, Netherlands. [9]Center for Infectious Disease Dynamics, The Pennsylvania State University, University Park, PA 16802, USA. [10]Department of Ecology and Evolutionary Biology and Woodrow Wilson School, Princeton University, Princeton, NJ 08540, USA.

*To whom correspondence should be addressed. Email: awpark@uga.edu